Product Distribution in the Photolysis of s-cis Butadiene: A Dynamics Simulation

Marco Garavelli,*,‡ Fernando Bernardi,‡ Massimo Olivucci,*,§ Michael J. Bearpark,† Stephane Klein,† and Michael A. Robb*,†

Department of Chemistry, King's College, London, Strand, London, UK WC2R 2LS, Dipartimento di Chimica "G. Ciamician", Università di Bologna, Via Selmi 2, 40126 Bologna, Italy, and Dipartimento di Chimica, Università di Siena, Via Aldo Moro, 53100 Siena

Received: May 31, 2001; In Final Form: August 20, 2001

In this paper, we report the results of nonadiabatic molecular dynamics computations on s-cis butadiene. Our objective was to understand the complex mechanism of the photolysis of this hydrocarbon through the analysis of an ensemble of trajectories computed with the hybrid MMVB method. Within the limitations of our computational strategy (the initial conditions and the limitations of the MMVB potential), our results suggest that some of the experimentally observed photoproducts such as s-trans butadiene, bicyclobutane, and *Z*,*Z*-butadienes (obtained by irradiating substituted *E*,*E*-butadienes) are exclusively formed through "dynamic paths" defined by certain subsets of trajectories that lie far from conventional minimum energy paths. In particular, concurrent double bond isomerization (e.g., *Z*,*Z*→*E*,*E* isomerization) seems to be achieved by decay of a "*dynamically locked intermediate*", a metastable excited-state species.

1. Introduction

Butadiene **1** represents a model for the photochemistry of conjugated dienes in general.[1−4] These compounds undergo several competing photochemical rearrangements, including *E*/*Z* (double bond) isomerization, s-cis/s-trans (single bond) isomerization, as well as cyclization to cyclobutenes (the textbook example for the Woodward−Hoffmann rules[5] for electrocyclic reactions) and bicyclization to bicyclobutanes.

Previously, we reported[4d−f] a detailed mapping of the spectroscopic ($1B_2$) and dark ($2A_1$) excited-state potential energy surfaces (PESs) controlling the photochemistry of s-cis butadiene (**1**) using ab initio CASSCF[6] optimized geometries and multiconfigurational perturbation theory (CASPT2)[7] energetics. These studies established that, after photoexcitation **1** evolves along barrierless reaction pathways (i.e., minimum energy paths, MEPs[8]), which ultimately lead to the different ground-state photoproducts. In particular, we located[4e] MEPs for the disrotatory formation of cyclobutene (**2**), for *E*/*Z* isomerization of one double bond (**$1_{E\rightarrow Z}$**) and the inefficient formation of a bicyclobutane (**3**) precursor, the methylenecyclopropyl 1,3-diradical (**4**) (see Figure 1 and Table 1 for the energetics). We also located a higher lying, barrier controlled, path leading to production of the conrotatory (W.-H. photochemically forbidden) product (see light lines in Figure 1). However, the mechanistic information derived from an MEP is structural (i.e., non dynamical) and provides chemical insight only for 'cold' photochemistry (i.e., vibrationally 'cold' excited states reactants, where slow motion is possible). Such information may be not sufficient for a description of photochemical reactivity. In particular, when the process of removal (or redistribution) of the vibrational excess energy is inefficient (e.g., in the gas phase, where the interaction with the solvent is absent) and slower than the reactive process, molecules may not follow the MEP valleys. The major consequence of such evolution is that the system will not decay to the ground state at the minimum energy of the conical intersection at the end of the MEP (or near it),[9] but rather at a different higher energy point on the intersection space. In such cases, a computational investigation of the excited-state/ground-state motion requires a dynamics treatment.

TABLE 1: S_1 Relative Energies at the MMVB (ΔE_{MMVB}), CASSCF/4-31G (ΔE_{CAS}), and CASPT2/DZ+spd Level (ΔE_{PT2}), for Selected s-cis-butadiene Structures, as Defined in Ref 4d[h]

structure[a]	ΔE_{MMVB} (kcal/mol)	ΔE_{CAS} (kcal/mol)	ΔE_{PT2}[a] (kcal/mol)
C_{2v}**-GS MIN**[b]	42.7[b]	40.4[b]	37.7[b]
C_S**-MIN**[c]	0.0	0.0	0.0
C_2**-MIN**[c]	0.5	1.3	3.8
C_{2v}**-MAX**[d]	4.0	5.1	10.2
C_S/C_2**-TS**[e]	1.4	2.0	4.2
C_S**/CI-TS**[f]	1.1	1.9	−0.8
C_2**/CI-TS**[f]	3.0	5.0	7.3
S_1/S_0 **CI**[g]	−4.0	−2.0	−3.9

[a] From ref 4d−e. [b] S_1 Franck−Condon region (ground-state equilibrium structure). [c] S_1 minima. [d] S_1 planar stationary point. [e] S_1 transition state connecting the two minima. [f] S_1 transition states leading to the lowest energy CI point. [g] Lowest energy CI point. [h] Here, we use the improved MMVB potential.

In recent years, there has been considerable interest in combining quantum mechanics with molecular mechanics (MM) to model the dynamics of large molecules. We have developed the hybrid approach MMVB (Molecular Mechanics−Valence Bond) based upon valence bond (VB) theory and linked to an MM force field[10,11] that enables excited-state processes to be modeled. MMVB is designed to reproduce the shape of the ab initio CASSCF potential surface for the ground and covalent excited states of conjugated hydrocarbons and all vibrational degrees of freedom of the molecule are considered. Although MMVB permits a study of the dynamics much more cheaply than ab initio methods, reaction barriers and excitation

† Department of Chemistry, King's College, London.
‡ Università di Bologna.
§ Università di Siena.

10.1021/jp012058l CCC: $20.00
Published on Web 12/04/2001

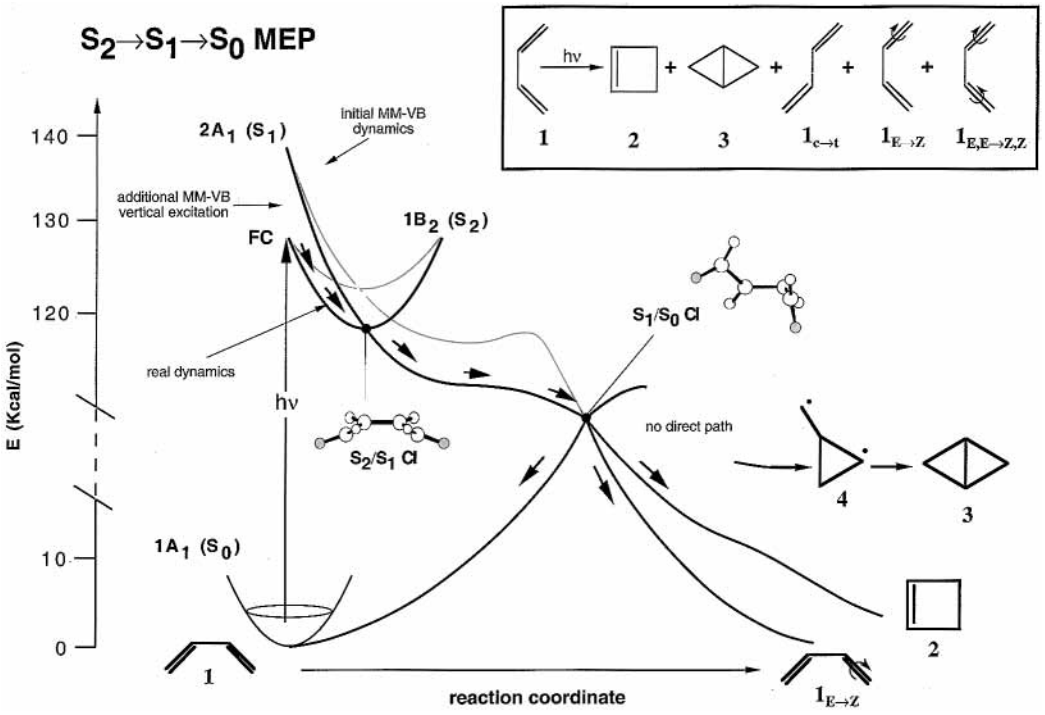

Figure 1. Schematic illustration of the previously reported [4c−e] ab initio MEPs for s-cis butadiene. Full lines and light lines represent the energy profile along the disrotatory and conrotatory excited-state MEP, respectively. Dark arrows qualitatively illustrate the "real" relaxation process following photoexcitation to the spectroscopic state $1B_2$ (S_2). Grey arrows describe the effective MMVB initial relaxation process out of the FC region on the covalent excited $2A_1$ (S_1) state: the additional vertical excitation energy included in MMVB dynamics simulations is shown. In the inset (top right) we show the whole spectrum of final primary photoproducts observed in s-cis butadiene photochemistry [1a]. Notice that, while direct reaction paths for $\mathbf{1}_{E,E\rightarrow Z,Z}$ $\mathbf{1}_{c\rightarrow t}$ and **3** photoformation do not exist, these photoproducts have indeed been observed.[1a]

energies are not obtained with quantitative accuracy. Accordingly, in this work we have improved the MMVB force field by re-fitting the MMVB potential *specifically* for s-cis butadiene. We must emphasize that even with these improvements to the energetics, our target is to obtain mechanistic information. Thus, our initial set of molecular configurations and momenta has been chosen in order to sample a wide range of physically interesting excited-state geometries rather than to generate statistically correct dynamics results.

Butadiene is a good prototype model for dynamics and reactivity studies because a large amount of data (both experimental[1a,2f] and theoretical[4a,4c−e,12]) are available for the photoisomerization process. Ito et al.[12d] investigated s-trans butadiene photoisomerization dynamics by means of a semiclassical surface hopping method using a parametrized model Hamiltonian. This study showed that nonadiabatic decay takes place at triply twisted CC conformations (conical intersection points) in agreement with our previous theoretical work.[4] The functional form for the model Hamiltonian used by Ito et al. used only a few degrees of freedom (i.e., CC bond stretching, bending and torsion). Thus, they were unable to study the full range of photoproducts. Recently, Domcke and co-workers[12f] simulated (via time-dependent wave packet calculations) the ultrafast (30fs) $1^1B_u \rightarrow 2^1A_g$ decay dynamics occurring, through a conical intersection point, in s-trans butadiene. Although MMVB simulations cannot address this initial part of the relaxation process (see section 2), nevertheless our unconstrained MMVB dynamics allows us to sample the full coordinate space and to get detailed mechanistic information on photoproducts formation for a given choice of initial conditions (see following discussion in section 2).

The static view for the s-cis butadiene radiationless decay process via a conical intersection (illustrated by means of the MEPs in Figure 1) shows that no accessible reaction paths exist for concomitant double bond isomerization ($\mathbf{1} \rightarrow \mathbf{1}_{E,E\rightarrow Z,Z}$), s-cis/s-trans interconversion ($\mathbf{1} \rightarrow \mathbf{1}_{c\rightarrow t}$), and the formation of the bicyclic intermediate (**1**→**3**). As we shall subsequently discuss, our MMVB based molecular dynamics simulation is able to account for the generation of all these compounds so that the whole spectrum of observed photoproducts can be reproduced (see inset in Figure 1). Moreover, despite the limitations of the MMVB potential (see section 2), a qualitative agreement between the simulated and observed quantum yield (QY) distribution[1a,d−g] has been achieved. Further, our simulations also indicate the existence of a novel mechanistic feature, a transient excited-state intermediate that does not correspond to a potential energy minimum, yet appears to play an important role (if vibrational excess energy removal is inefficient) in determining the excited-state lifetimes and photoproduct distribution.

2. Computational Details

MMVB Force Field Improvement. In our dynamics simulation, the energy and gradients are computed within the hybrid molecular-mechanics/valence-bond MMVB method.[10] This method uses a parametrized Heisenberg Hamiltonian[11] to represent the quantum mechanical part in a VB space. A basic set of VB parameters (exchange (K) and coulomb (Q) integrals)[10a] have been fitted to ab initio CASSCF data (4-31G basis set) for two-active-center model molecules (ethane and ethylene) for modeling σ and π C−C bonds. A delocalization algorithm is used to yield a general MMVB algorithm. This delocalization algorithm has been parametrized against a more general "training set" of multi-active-center systems (see ref 10a for a full detailed description of the method). In the present computations, the delocalization algorithm has been re-parametrized against a sample of geometries for butadiene alone to yield a force field that is much more accurate but applicable only to butadiene

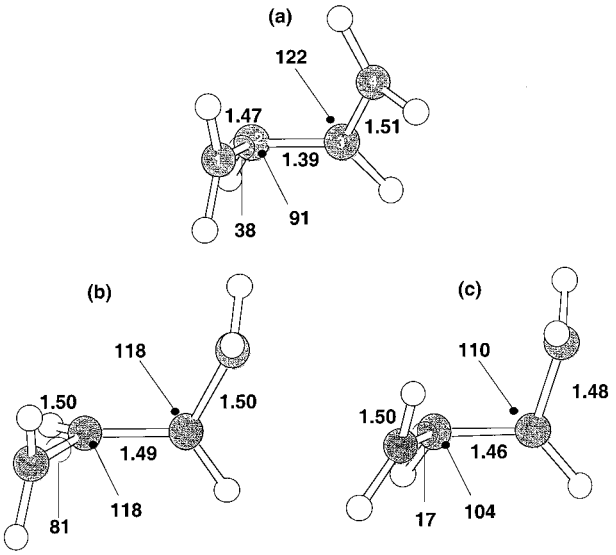

Figure 2. (a) CASSCF/4-31G and (b−c) MMVB optimized conical intersection geometry for s-cis butadiene with the old (b) and the new (c) set of parameters. Bond distances are given in Å. Bending and twisting angles are given in degrees.

(see the related methodological paper). In particular, an ab initio CASSCF/4-31G S_1 surface based upon a grid of points around the excited-state key structures (the points shown in Table 1: the excited-state minima, transition states and the lowest energy point on the conical intersection) has been used for the fitting procedure. The new fitted MMVB potential[13] results in an improved description for the topology and energetics of the excited S_1 state when compared to the CASSCF/4-31G surface (see Table 1). The optimized geometry for the low energy crossing point obtained with the re-parametrized MMVB (Figure 2c) is now similar to the ab initio structure (Figure 2a), except for the central C−C bond length which is still longer, although shorter than the old MMVB structure (see Figure 2b). Similarly, the nonadiabatic coupling vector is well reproduced, with its major components involving bicyclobutane formation (i.e., the bending of the angle C1−C2−C3) with primarily disrotatory CH_2 motion. In addition, the previously computed S_0 ab initio MEPs[4e] departing from the lowest energy crossing point (see Figure 1) are now reproduced at the MMVB level, including ring formation paths. This improved MMVB potential has been used for the dynamics simulations reported in this work.

Although our improved (re-parametrized) MMVB method gives results (for both geometries and relative energetics) in much better agreement with the reference ab initio (CASSCF/4-31G) surface, there remain significant differences from the most accurate potential. Table 1 reports the S_1 energy values computed at different computational levels (the MMVB, the reference CASSCF/4-31G, and the most accurate CASPT2 as previously reported in ref 4d), for the relevant excited-state points involved in s-cis butadiene photochemistry. In particular, it should be noticed that, although MMVB (and partly also CASSCF/4-31G) gives two almost energetically equivalent disrotatory and conrotatory paths (via ***C*$_S$/CI-TS** and ***C*$_2$/CI-TS** transition states respectively), at the CASPT2 level the computed disrotatory route is barrierless (i.e., a *negative* energy barrier value) and thus much more favored than the corresponding conrotatory one, which involves a ca. 7 kcal/mol barrier (see dark and light lines in Figure 1). Despite these quantitative differences, as we shall show, our MMVB dynamics reproduces the complete photoproduct spectrum with a substantial agreement between simulated and observed QY distribution.

Dynamics and Choice of Initial Conditions. We now address the choice of the initial sample of molecular configurations and momenta in the Franck−Condon (FC) region. First, we must emphasize that MMVB can only describe covalent (not ionic) states. Consequently, we can only study the ground (S_0) and covalent (S_1) excited states in butadiene and the initial ultrafast dynamics on the spectroscopic (bright) ionic S_2 state (whose decay occurs in tens of femtoseconds[2n,12f]) cannot be modeled (see dark arrows schematically represented in Figure 1). Accordingly, our trajectories are initiated on the covalent (dark) excited S_1 state. Thus, this procedure neglects the effect of S_2 state dynamics on stereochemistry, lifetimes, etc. Moreover, in selecting initial conditions, the excitation energy used is ∼10 kcal/mol in excess of the vertical excitation energy to allow for the fact that the dark S_1 state is higher laying than the spectroscopic S_2 state in the FC region (see gray arrows in Figure 1).

To define the starting conditions for the excited-state trajectories to be run, we have simulated the "photoexcitation" process for s-cis butadiene[14b] using classical ideas. To generate the starting set of geometries and momenta, we have run a 1.5 ps trajectory on S_0 with 56 kcal/mol excess energy (with respect to the absolute minimum on S_0). We then choose initial geometries and momenta from this trajectory after allowing time (∼200 fs) for intramolecular vibrational energy redistribution (IVR) and equilibration between kinetic and potential energy (so as to satisfy the virial theorem). We have chosen as starting points for excited-state dynamics those points of the S_0 trajectory with a S_1-S_0 energy gap of 171 kcal/mol (i.e., the vertical MMVB $S_0 \rightarrow S_1$ excitation energy computed at the geometry of the ground-state minimum) ± 5 kcal/mol (i.e., an energy spread to allow for wavelength broadening). A batch of 250 excited-state (S_1) trajectories is then run (for 1−2 ps) using these starting conditions. We recognize that this sample biases the importance of low-frequency ground-state vibrations (i.e., torsions and bends) relative to higher frequency stretches.[15] However, our objective is primarily to demonstrate the existence of "reaction channels" that would not have been predicted from a study of the MEP alone. Thus, our sampling method should be seen as an ad hoc procedure for generating initial conditions that will sample wide regions of the excited-state potential surface.

The dynamics method used employs a "direct" procedure for solving the equations of motion (i.e., the gradient that drives the dynamics is evaluated "on the fly") and thus one avoids the tedious, and often unfeasible, parametrization of an analytical expression of a multidimensional energy surface.[16] The trajectory-surface-hopping (TSH) algorithm of Tully and Preston[17] has been used to propagate excited-state trajectories onto the ground state in the region of a conical intersection (see refs 10e−f and 18 for examples and applications). However, surface hop approaches are not very well-defined for the case where the trajectory re-crosses the region of strong coupling many times.[14c−d] This problem occurs in the case of a sloped intersection.[14b] We have recently implemented[14b] a new approach that uses mixed state (MX-ST) dynamics (first used with a diatomics-in-molecules model by Gadea and co-workers[14a]). Here the nuclear dynamics are controlled by the *Ehrenfest* force (i.e., the gradient is computed directly from time dependent CI wave function). Thus, the trajectory "feels" both potential surfaces and the nonadiabatic couplings all the time. We have run our simulations with both methods and the results are essentially the same because the surface hops are always

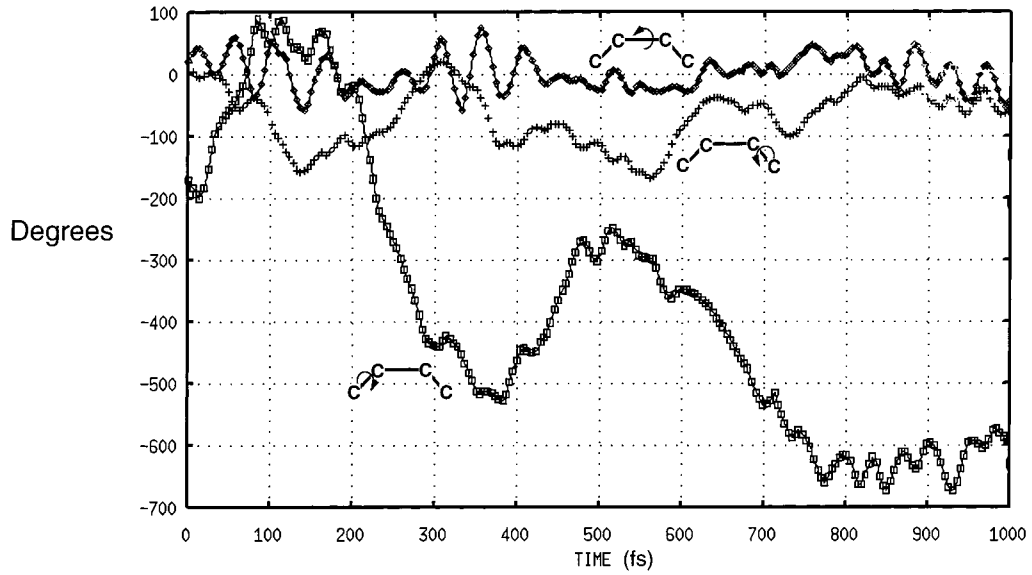

Figure 3. Skeletal twisting of s-cis butadiene vs time (fs) for a prototype long-living trajectory. The three plots represent the values (in degrees) of the dihedral angles associated with the twisting around the central C−C bond and the two external C−C bonds. The planar s-cis butadiene reactant corresponds to values of 0°, 0° and −180° for the central and the two external dihedral angles, respectively. Values out of the range [−360°, +360°] indicates multiple clockwise (−)/anticlockwise (+) rotations around C−C bonds.

TABLE 2: Experimental and Simulated QY Photoproduct Distribution[a]

photoproducts[b]	exp QY[c] (%)	simulated QY[d] (%)
2	**4−12**[e]	<**24**[f]
3	**0.4−1.2**[g]	<**2**
$\mathbf{1}_{E\rightarrow Z}$[h]	**36−46**[i]	41
$\mathbf{1}_{E,E\rightarrow Z,Z}$[h]	<**2**[l]	14

[a] Both the experimental and the computed QYs do not add up to 100% because the reported values are only over the detected photoproducts **2**, **3**, $\mathbf{1}_{E\rightarrow Z}$, and $\mathbf{1}_{E,E\rightarrow Z,Z}$ (i.e., different isomers of the starting reactant **1**), while reactant back formation is not reported. The QY for the unisomerized system (**1**) may be simply evaluated by difference. [b] See Figure 1 for a definition of the photoproduct labels used here. [c] Experimentally observed QY, see ref 1a,d−g. [d] Trajectory−Surface−Hopping calculated QY. [e] Only disrotatory **2** is observed, see ref 1a,d−f. [f] Half disrotatory (12%) and half conrotatory (12%) cyclobutene build up the overall QY for **2**. [g] QY for **3** has been estimated as 1/10 of the observed one for **2**, see ref 1a,g. [h] For all trajectories leading back to butadiene (regardless these lead either to **1**, or to $\mathbf{1}_{E\rightarrow Z}$, or to $\mathbf{1}_{E,E\rightarrow Z,Z}$ formation) free rotation about the central C−C bond has been observed. This is due to the excess vibrational energy found in our simulation conditions, which leads to s-cis/s-trans thermal equilibration (see the discussion at the end of section 3). [i] Ref 1a,e−f. [l] Ref 1a,e.

TABLE 3: S_1 Lifetimes (τ_{S_1}) for the Computed Trajectories

lifetimes	% of trajectories[a]
$\tau_{S_1} < 300$ fs	63
$\tau_{S_1} > 500$ fs ($\tau_{S_1} > 1$ ps)	16 (5)

[a] Simulation at the Trajectory-Surface-Hopping level.

effectively instantaneous and essentially diabatic in nature. Accordingly we report only the TSH results.

3. Results and Discussion

Our computed quantum yields and lifetimes are given in Tables 2 and 3. A photoproduct QY (see Table 2) has been calculated as the fraction of the total number of trajectories hopping onto S_0, which subsequently enters a specific ground-state energy well (i.e., the photoproduct minimum). Therefore, in the total count we neglect those trajectories which are still on S_1 at the end (2 ps) of the dynamics simulation (5% and 7% of the TSH and MX-ST trajectories respectively never decay). The excited-state (S_1) lifetime for a trajectory (τ_{S_1}, see Table 3) is given by the time spent by that trajectory on S_1 (before decay occurs).

We shall structure the discussion of our results around two mechanistic findings: (i) the formation of a "*dynamically locked intermediate*", i.e., a species with a finite lifetime that does not correspond to an energy minimum on S_1; (ii) the existence of trajectories lying far from MEPs (which we shall call " dynamic reaction paths"). We conclude the section with a comparison of simulated and experimental QYs.

(i) A Dynamically Locked Intermediate. In this subsection, we discuss the unexpected high QY (14%) calculated for the **1** → $\mathbf{1}_{E,E\rightarrow Z,Z}$ process (see Table 2). The experimental QY is less than 2% (in the condensed phase).

The analysis of the longer living excited-state trajectories (e.g., ≥ 1ps) reveals formation of an excited-state species that does not correspond to an energy minimum on either S_1 or S_0. In fact, ca. 5% of the trajectories (Table 3) lead to an S_1 geometry that has essentially an s-cis planar-backbone configuration, where the system is trapped in "orbits" with rotating methylenes and oscillating C−C bonds, without decaying onto the ground state. Here, the S_1/S_0 energy gap separation is always greater than 13 kcal/mol, while the S_1 energy is always well above the optimized S_1 minimum (***C*****$_S$-MIN**, see Table 2). Figures 3−5 document the behavior of this species along one of the longer living S_1 trajectories. The rotation of the two terminal methylenes is almost free (see plot 2 and 3 in Figure 3), whereas the twisting of the central bond (plot 1) is hindered (due to its partial double-bond character). This fact is also evident from Figure 4 where vibrations for C−C bond lengths are shown. The central C−C bond has a mean length of 1.49 Å (see Figure 4a), whereas the external C−C methylene bonds are longer (1.54 Å, see Figure 4b,c). Thus, one has partial single-double bond inversion, as expected for the S_1 state of a polyene. Snapshots from the same trajectory are shown in Figure 5. Here, one can observe the almost planar carbon skeleton with rapidly twisting terminal methylenes.

Because of the formation of this locked intermediate, the gas-phase dynamics of s-cis butadiene should result in longer τ_{S_1} (see Table 3) and enhanced fluorescence QY as compared to

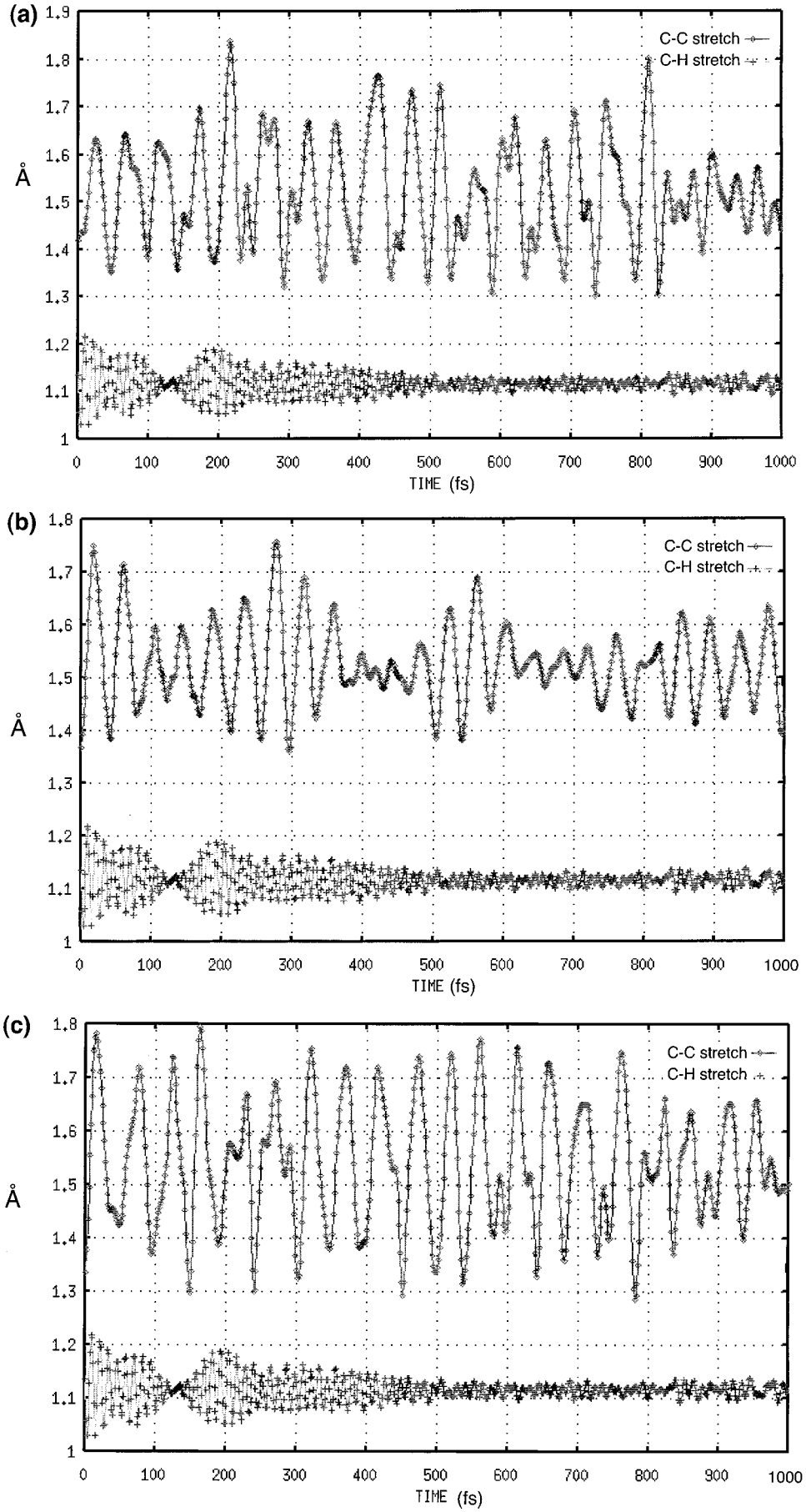

Figure 4. C−C stretching oscillations (in Å) vs time (fs) along a prototype long-living trajectory (see Figures 3). The C−C stretch plot displays the (a) central C−C bond and (b−c) external C−C bonds oscillations. The corresponding C−H bond oscillation has been reported in diagrams (a−c) for comparison.

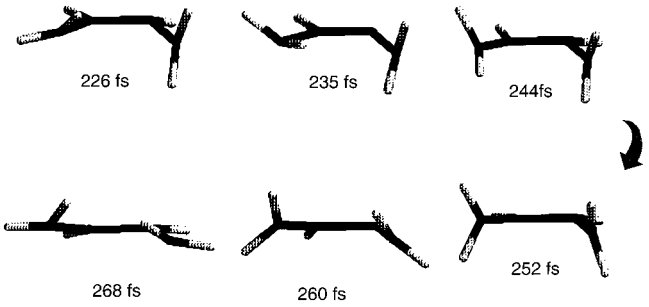

Figure 5. Snapshots of the molecular structure along the prototype long-living trajectory (see Figures 3) showing methylenes free rotation and an almost planar s-cis carbon skeleton.

s-cis butadiene in condensed phase.[2f] Consequently, a higher QY for double isomerization **1** → $\mathbf{1}_{E,E\rightarrow Z,Z}$ should also be observed (see Table 2). No gas-phase experiments on s-cis butadiene exist to prove our conclusions. Recent observations on the gas phase (molecular beam) photochemistry of allyl radicals[19] seem to reveal an unexpectedly long excited-state lifetime (i.e., ps time scale). Because we have previously provided evidence[4a] that photoexcited allyl radicals evolve along a barrierless reaction path (MEP) ending at a conical intersection funnel as it happens for **1**, the long excited-state lifetime could be due to a dynamic effect such as the one described above for s-cis butadiene.

Removal of excess vibrational energy (e.g., by the solvent in condensed phase) inhibits the formation of this dynamically locked species. We have simulated this effect using a simple viscosity algorithm. At each step of the trajectory the momentum was reduced (by using a scaling factor) according to Stokes law.[20] The dissipation of vibrational energy to the environment invariably caused a decrease of S_1 lifetime (τ_{S_1}) for all trajectories consistent with the experimentally observed ultrafast excited-state relaxation of butadiene in solution.[2f] In this case, due to energy dissipation, trajectories become more and more close to the barrierless MEP (see Scheme 1) leading to the low energy CI (see Figure 2) and to ultrafast nonadiabatic transitions. Moreover, because a decrease in τ_{S_1} occurred concurrently with the decrease in the calculated **1** → $\mathbf{1}_{E,E\rightarrow Z,Z}$ QY, we suggest that the dynamically locked intermediate is the precursor of the **1** → $\mathbf{1}_{E,E\rightarrow Z,Z}$ reactive process.[21]

(ii) Dynamic Reaction Paths. We begin with an analysis of the hopping geometries (i.e., the points where $S_1 \rightarrow S_0$ decay occurs). Because conical intersection points form a *n*-2-dimensional subspace (i.e., an hyperline) of the full (*n* dimensional) hyperspace of the vibrational degrees of freedom, the surface crossing can occur in regions far away from the optimized conical intersection.

Figure 6 shows three surface crossing geometries along three representative trajectories leading to bicyclobutane (**3**), cyclobutene (**2**), and butadiene (**1**), respectively. At the crossing point the structure appears to be "biased" toward the ultimate photoproduct structure. For example, the crossing point leading to the diradical **4** (a ground-state intermediate precursor to **3**, see Figure 6a) has one very small C−C−C angle and two rotated methylenes. This arrangement favors the correct overlap between the carbon p orbitals in position 1 and 3. Similarly, for the case of cyclobutene generation, the geometry at the crossing point (Figure 6b) is arranged in order to maximize the 1−4 interaction and four-membered ring closure. Finally, the crossing point for a trajectory (Figure 6c) leading back to reactant **1** has longer 1−3 and 1−4 C−C distances, larger C−C−C bending angles, and the methylenes twisted in such a way that ring closure interactions are inhibited (see Figure 6c).

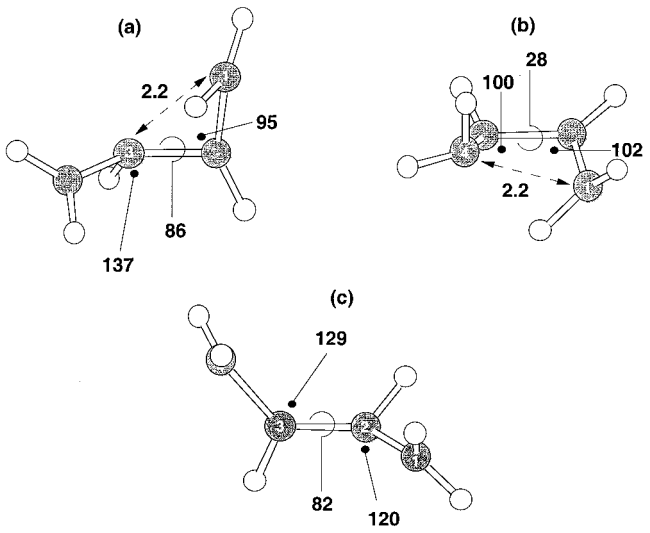

Figure 6. (a) Typical hopping geometries along three (TSH) trajectories leading to (a) bicyclobutane, (b) cyclobutene and (c) butadiene. Bond distances are given in Å. Bending and twisting angles are given in degrees.

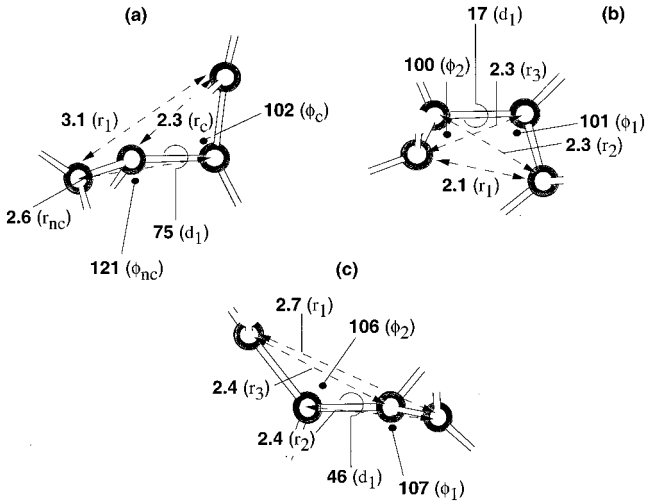

Figure 7. Mean values of some relevant geometrical parameters for hopping geometries leading to (a) **3**, (b) **2** and (c) **1** (the symbols used for the discussion in the text are given in brackets). Subscripts **c** and **nc** refers to the three-membered ring formation process (cyclopropanation) occurring at bicyclobutane generating hopping points: **c** refers to the closing C−C−C bending angle leading to cyclopropane and **nc** refers to the nonclosing one. Bond distances are given in Å. Bending and dihedral angles are given in degrees.

The conjecture that the molecular structure at the surface crossing point on the trajectory partly determines the photoproduct is supported by a more systematic analysis of the surface crossing geometries in the computed trajectories. The results of this analysis are shown in Figures 7 and 8. Hopping structures of trajectories leading to **3** (see Figure 7a) have a very small (∼102°) mean value for the C−C−C bending angle ϕ_c (i.e., the closing angle to yield the diradical precursor **4**), whereas the other (the nonclosing angle, ϕ_{nc}) is much larger (∼121°). The same trend is observed for C−C distances and dihedral angles, where both the 1,4 C−C distance (r_1) and the C1−C2−C3−C4 dihedral angle (d_1) have a large mean value (3.1 Å and 75°). In contrast, the closing 1,3 C−C distance (r_c) is smaller (2.3 Å) than the nonclosing (r_{nc}) one (2.6 Å). Along the trajectories leading to **2** the hop structures (see Figure 7b) have very small mean values for the relevant C−C−C bending angles (101° and 100° for ϕ_1 and ϕ_2), as well as for d_1 (17°) and r_1, r_2,

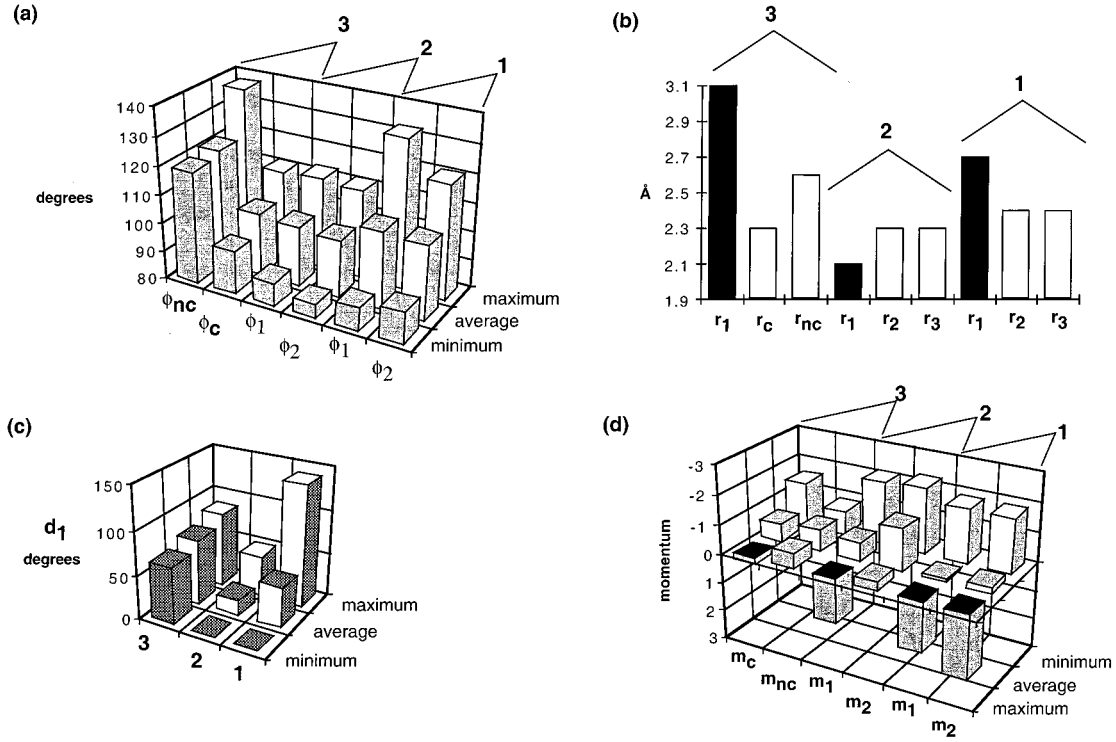

Figure 8. Analysis of the hopping geometries (from TSH trajectories). (a−c) Hopping geometries leading to the bicyclobutane, cyclobutene, and butadiene photoproducts are labeled as **3**, **2**, and **1**, respectively. The corresponding geometrical parameters are defined in Figure 7. (d) Statistical analysis of the main components of the momentum at the hopping geometries: m_1 and m_2 (or m_c and m_{nc}) describe the opening or closure (positive or negative sign respectively) of the C−C−C bending angles ϕ_1 and ϕ_2 (or ϕ_c and ϕ_{nc}) as described in Figure 7. The spread (i.e., the maximum and minimum values) for the parameters analyzed is also shown.

and r_3 (2.1, 2.3, and 2.3 Å respectively). Finally, hop points leading to butadiene back-formation (**1**) (see Figure 7b) have larger mean values for ϕ_1 and ϕ_2 (107° and 106°), d_1 (46°) and r_1, r_2, and r_3 (2.7, 2.4, and 2.4 Å respectively). Bar diagrams in Figure 8a−c summarize these results and display the spread for the geometrical parameters discussed in the text.

A certain number of hop structures have been identified which, although having a geometry biased toward a specific photoproduct, ultimately reach a different photoproduct well (notice the spread—maximum and minimum—for the parameters analyzed in Figure 8a,c). This is because the momentum developed along the excited-state branch of the trajectory drives the system out of the expected photoproduct channel. Figure 8d (to be examined in conjunction with Figure 8a) summarizes the results for the two most important components of the momentum at the decay points, i.e., m_1 and m_2 (or m_c and m_{nc}). These components describe momentum in the opening (positive sign) or closure (negative sign) of the two C−C−C bending angles ϕ_1 and ϕ_2 (or ϕ_c and ϕ_{nc}), see Figure 7. Figure 8d shows how a dynamic effect must act in concert with the geometric effect analyzed above. Bicyclobutane, cyclobutene, or butadiene photogeneration occurs if the momentum prompts a motion that is coupled with the geometry at the hop. Thus, negative values (describing bending angle closure) favor ring closure reactions to bicyclobutane or cyclobutene (see the negative mean values for both components leading to **3** or **2**), whereas positive or randomly distributed ones favor butadiene back formation (m_1 and m_2 mean values to **1** are almost zero, while a huge spread, indicative of random positive and negative values, is observed).

In summary, these results show that both geometric and dynamic effects (i.e., hop structures and momenta) operate in the selection of ground-state reaction/relaxation paths in isolated conditions. Structural factors alone (i.e., MEPs) seem to dominate the relaxation process when friction (e.g., a viscosity effect) or vibrational energy removal is active

Simulated and Experimental Quantum Yields. The relative quantum yields for **3** and $\mathbf{1}_{E\rightarrow Z}$ photogeneration are qualitatively reproduced by our simulation (see Table 2), whereas the QY for $\mathbf{1} \rightarrow \mathbf{2}$ and $\mathbf{1} \rightarrow \mathbf{1}_{E,E\rightarrow Z,Z}$ processes are not in good agreement with observations.

In previous works, we have shown that the observed disrotatory stereoselectivity of the ring-closure reaction ($\mathbf{1} \rightarrow \mathbf{2}$) can be rationalized by taking into account energetic and dynamic factors.[4d−e] In fact, evolution along an asymmetric disrotatory route on S_1 is barrierless, whereas the evolution along an alternative conrotatory route involves overcoming a ca. 7 kcal/mol barrier (see CASPT2 barriers in Table 1 and Figure 1). Moreover, the initial relaxation on the spectroscopic state accelerates the system toward the favored S_1 disrotatory path. This effect has been recently simulated by Martinez et al.[14f] for cyclobutene, which shows an initial ultrafast (∼15fs) relaxation out of the FC region on the spectroscopic state involving an immediate disrotatory ring-opening motion. Our simulation fails to predict the observed disrotatory stereoselectivity. Rather, photoproduct **2** distribution is 50% disrotatory and 50% conrotatory (see note f in Table 2). This is due, in part, to the fact that our simulations neglect the dynamics of the spectroscopic state (see section 2). However, the main reason for this discrepancy is that the improved MMVB surface has almost energetically equivalent disrotatory and conrotatory routes (see Table 1), so there is no energetic factor controlling the selectivity. Thus, our computed QY for the four-membered ring-closure reaction to give **2** (i.e., considering both conrotatory and disrotatory processes) is twice the experimental value, as shown in Table 2 (notice how only the $\mathbf{1} \rightarrow \mathbf{2}_{\mathbf{disrotatory}}$ QY is well reproduced).

The most serious disagreement concerns QY for the $\mathbf{1} \rightarrow \mathbf{1_{E,E \rightarrow Z,Z}}$ process. One can rationalize these observations recognizing that the experimental data are for the condensed phase (i.e., solution and cold matrices). In fact, it has been recently shown, both computationally[22] and experimentally,[23] that efficient energy transfer to the solvent is already active on the subpicosecond time scale.[24] In our simulations there is no energy loss to the surroundings. Consequently, no energy dissipation is active and excess vibrational energy is accumulated on the excited state before decay. Because partial single/double bond inversion occurs on S_1 (as previously shown), the double isomerization is unhindered in long living excited-state trajectories (i.e., the dynamically locked species) and methylenes can rotate almost freely (as already discussed). Thus, the disproportionate QY for concurrent double-bonds isomerization ($\mathbf{1} \rightarrow \mathbf{1_{E,E \rightarrow Z,Z}}$) is a consequence of those long living excited state trajectories which would not exist in condensed phase. The same phenomenon has been recently simulated on S_0 for the dynamics of longer polyenes,[25] and this is the second computational evidence of such a dynamic feature (i.e., a metastable species) found in polyene dynamics.

Following decay onto S_0 even more excess vibrational energy is accumulated into the system if friction effects are absent. This results in a mean value for the excess vibrational energy of ~10 kcal/mol per degree of freedom. This energy is higher than the conformational barrier to s-cis/s-trans isomerization (~5 kcal/mol), so that free rotation about the central single bond is observed along ground-state trajectories and the s-cis/s-trans conformers of **1** may freely interconvert. Thus, in our simulation conditions, thermal equilibration between the two conformers can occur in contrast with the small QY for the $\mathbf{1} \rightarrow \mathbf{1_{c \rightarrow t}}$ process observed in condensed phase (experiments in cold matrix give a QY for $\mathbf{1_{c \rightarrow t}}$ slightly larger than the one observed for **2**, i.e., $\geq 4\%$[1a]).

As discussed above, when a perturbation such as a viscosity effect is switched on, the simulated τ_{S_1} and QY for the $\mathbf{1} \rightarrow \mathbf{1_{E,E \rightarrow Z,Z}}$ process drop down concurrently due to the dissipation (cooling) of excess vibrational energy to the environment. At the same time, thermal s-cis/s-trans equilibration is hindered and a less efficient $\mathbf{1} \rightarrow \mathbf{1_{c \rightarrow t}}$ process occurs, in line with the results observed in condensed phase. This finding provides a validation of our interpretation, that excess undissipated vibrational energy is the source of the differences between condensed phase and hot gas phase photodynamics, guaranteeing the existence of dynamically locked species on S_1.

4. Conclusions

In this paper, we have shown how semiclassical dynamics with an improved MMVB potential can be used to investigate the mechanism of an "elementary" photochemical reaction in the gas-phase. In contrast to previous attempts to describe butadiene dynamics (based on approximated Hamiltonians and constrained spaces of reduced degrees of freedom),[12d] we have performed systematic full-unconstrained dynamics computations, which reproduce the full photoproduct spectrum of **1** with a qualitative agreement between the simulated and observed QY distribution. A new feature of butadiene dynamics emerges which corresponds to a "metastable" excited-state species with a relatively long excited-state lifetime (≥1 ps time scale). Because no direct experimental observations are available for gas phase s-cis butadiene dynamics, our study provides a prediction for gas phase toward solvent/matrix-dependent photochemistry.

References and Notes

(1) (a) Leigh, W. J. In *CRC Handbook of Organic Photochemistry and Photobiology*; Horspool, W. M., Song, P.-S., Eds.; CRC Press: 1995; pp 123−142 and references therein. (b) Laarhoven, W. H.; Jacob, H. J. C. *ibid.* 143−154. (c) Kohler, B. *Chem. Rev.* **1993**, *93*, 41. (d) Boue, S.; Rondelez, D.; Vanderlinden, P. In *Excited states in Organic Chemistry and Biochemistry*; Pullman, B., Goldblum, N., Eds.; D. Reidel, Dordrecht, 1977; 199. (e) Saltiel, J.; Metts, L.; Wrighton, M. *J. Am. Chem. Soc.* **1970**, *92*, 3227. (f) Srinivasan, R. *J. Am. Chem. Soc.* **1962**, *84*, 4141. (g) Srinivasan, R.; Sonntag, F. I. *J. Am. Chem. Soc.* **1965**, *87*, 3778.

(2) (a) Petek, H.; Bell, A. J.; Christensen, R. L.; Yoshihara, K. *J. Chem. Phys.* **1992**, *96*, 2412. (b) Hayden, C. C.; Chandler, D. W. *J. Phys. Chem.* **1995**, *99*, 7897−7903. (c) Fuss, W.; Lochbrunner, S.; Muller, A. M.; Schikarski, T.; Schmid, W. E.; Trushin, S. A. *Chem. Phys.* **1998**, *232*, 161. (d) Cyr, D. R.; Hayden, C. C. *J. Chem. Phys.* **1996**, *104*, 771−774. (e) Ohta, K.; Naitoh, Y.; Saitow, K.; Tominaga, K.; Hirota, N.; Yoshihara, K. *Chem. Phys. Lett.* **1996**, *256*, 629. (f) Vaida, V. *Acc. Chem. Res.* **1986**, *19*, 114−120. (g) Petek, H.; Bell, A. J.; Christensen, R. L.; Yoshihara, K. *SPIE* **1992**, *1638*, 345−356. (h) Petek, H.; Bell, A. J.; Choi, Y. S.; Yoshihara, K.; Tounge, B. A.; Christensen, R. L. *J. Chem. Phys.* **1993**, *98*, 3777−3794. (i) Ashfold, M. N. R.; Clement, S. G.; Howe, J. D.; Western, C. M. *J. Chem. Soc., Faraday Trans.* **1993**, *89*, 1153−1172. (l) Muller, A. M.; Lochbrunner, S.; Schmid, W. E.; Fuss, W. *Angew. Chem., Int. Ed.* **1998**, *37*, 505. (m) Trulson, M. O.; Mathies, R. A. *J. Phys. Chem.* **1990**, *94*, 5741.

(3) (a) Saltiel, J.; Sears, D. F., Jr.; Ko, D.-H.; Park, K.-M. In *CRC Handbook of Organic Photochemistry and Photobiology*; Horspool, W. M., Song, P.-S. Ed.; CRC Press: 1995; pp 3−15. (b) Liu, R. S. H. *ibid.* pp 165−172. (c) Yoshizawa, T.; Kuwata, O. In *CRC Handbook of Organic Photochemistry and Photobiology*; Horspool, W. M., Song, P.-S., Eds.; CRC Press 1995; pp 1493−1499. (d) Rothschild, K. J.; Sonar, S. In *CRC Handbook of Organic Photochemistry and Photobiology*; Horspool, W. M., Song, P.-S., Eds.; CRC Press 1995; pp 1521−1544.

(4) (a) Celani, P.; Garavelli, M.; Ottani, S.; Bernardi, F.; Robb, M. A.; Olivucci, M. *J. Am. Chem. Soc.* **1995**, *117*, 11584. (b) Garavelli, M.; Celani, P.; Yamamoto, N.; Bernardi, F.; Robb, M. A. *J. Am. Chem. Soc.* **1996**, *118*, 11 656. (c) Garavelli, M.; Celani, P.; Bernardi, F.; Robb, M. A.; Olivucci, M. *J. Am. Chem. Soc.* **1997**, *119*, 11 487−11 494. (d) Celani, P.; Bernardi, F.; Olivucci, M.; Robb, M. A. *J. Chem. Phys.* **1995**, *102*, 5733. (e) Bernardi, F.; Olivucci, M.; Robb, M. A. *Chem. Soc. Rev.* **1996**, *25*, 321. (f) Garavelli, M.; Frabboni, B.; Fato, M.; Celani, P.; Bernardi, F.; Robb, M. A.; Olivucci, M.; *J. Am. Chem. Soc.* **1999**, *121*, 1537.

(5) Gilbert, A.; Baggot, J. in *Essentials of Molecular Photochemistry*, Blackwell Scientific Publications: Oxford, 1991.

(6) Roos, B. O. *Adv. Chem. Phys.* **1987**, *69*, 399−446.

(7) Andersson, K.; Malmqvist, P. A.; Roos, B. O. *J. Chem. Phys.* **1992**, *96*, 1218.

(8) Truhlar, D. G.; Steckler, R.; Gordon, M. S. *Chem. Rev.* **1987**, *87*, 217. Truhlar, D. G.; Gordon, M. S. *Science* **1990**, *249*, 491.

(9) (a) Klessinger, M. *Angew. Chem., Int. Ed. Engl.* **1995**, *34*, 549. (b) Michl, J.; Bonacic-Koutecky, V. *Electronic Aspects of Organic Photochemistry*; Wiley: New York, 1990.

(10) (a) Bernardi, F.; Olivucci, M.; Robb, M. A. *J. Am. Chem. Soc.* **1992**, *114*, 1606. (b) Smith, B. R.; Bearpark, M. J.; Robb, M. A.; Bernardi, F.; Olivucci, M. *Chem. Phys. Lett.* **1995**, *242*, 27. (c) Bearpark, M. J.; Bernardi, F.; Olivucci, M.; Robb, M. A. *Chem. Phys. Lett.* **1994**, *217*, 513. (d) Bearpark, M. J.; Bernardi, F.; Olivucci, M.; Robb, M. A. *J. Phys. Chem. A.* **1997**, *101*, 8395. (e) Bearpark, M. J.; Bernardi, F.; Clifford, S.; Olivucci, M.; Robb, M. A.; Smith, B. R. *J. Am. Chem. Soc.* **1996**, *118*, 169. (f) Bearpark, M. J.; Bernardi, F.; Olivucci, M.; Robb, M. A.; Smith, B. R. *J. Am. Chem. Soc.* **1996**, *118*, 5254.

(11) (a) Said, M.; Maynau, D.; Malrieu, J. P.; Bach, M. A. G. *J. Am. Chem. Soc.* **1984**, *106*, 571. (b) Maynau, D.; Durand, P.; Daudey, J. P.; Malrieu, J. P. *Phys. Rev. A*, **1983**, *28*, 3193. (c) Durand, P.; Malrieu, J. P. In *Adv. Chem. Phys. (Ab initio Methods in Quantum Chemistry* -I): Lawley, K. P., Ed.; John Wiley & Sons: Ltd., New York, 1987; Vol. 67, pp 321−412.

(12) (a) Aoyagi, M.; Osamura, Y.; Iwata, S. *J. Chem. Phys.* **1985**, *83*, 1140. (b) Zerbetto, F.; Zgierski, M. Z. *J. Chem. Phys.* **1990**, *93*, 1235. (c) Ohmine, I. *J. Chem. Phys.* **1985**, *83*, 2348. (d) Ito, M.; Ohmine, I. *J. Chem. Phys.* **1997**, *106*, 3159. (e) Buma, W. J.; Zerbetto, F. *Chem. Phys. Lett.* **1998**, *287*, 275. (f) Krawczyk, R. P.; Malsch, K.; Hohlneicher, G.; Gillen, R. C.; Domcke, W. *Chem. Phys. Lett.* **2000**, *320*, 535.

(13) Formulas and fitted parameters for the model σ (ethane) and π (ethylene) coulomb Q^0_{ij} and exchange K^0_{ij} integrals have not been modified. The same applies for the standard MM2 potential (involving not active atoms) and the modified MM potential (involving active atoms) used in MMVB (see ref 10a for a full detailed description of the method). The new set of s-cis butadiene parameters (used for the delocalization algorithm) was obtained via a standard least-squares fitting procedure. These parameters (g_1, h_1, g_2, h_2, e, f, s_1, s_2, s_3, t_1, t_2, t_3, and u, see ref 11a) have the values of 0.675 432, 1.025 067, 0.4390 414, 0.2, −0.316 717, 6.2304, 0.2, 7.0, −0.41,

0.27, 7.0, −0.34 and 10.342 464. The methodological paper with all the details on this fitting procedure is in preparation.

(14) (a) Amarouche, M.; Gadea, F. X.; Durup, J. *Chemical Physics* **1989**, *130*, 145. (b) Klein, S.; Bearpark, M. J.; Smith, B. R.; Robb, M. A.; Olivucci, M.; Bernardi, F. *Chem. Phys. Lett*, **1998**, *293*, 259. (c) Rose, T. S.; Rosker, M. J.; Zewail, A. H. *J. Chem. Phys.* **1989**, *91*, 7415. (d) Rosker, M. J.; Dantus, M.; Zewail, A. H. *J. Chem. Phys.* **1989**, *91*, 6113. (e) Martinez, T. J.; Ben-Nun, M.; Askenazi, G. *J. Chem. Phys.* **1996**, *104*, 2847. (f) Martinez, T. J.; Ben-Nun, M.; Levine, R. D. *J. Phys. Chem.* **1996**, *100*, 7884. (g) Ben-Nun, M.; Martinez, T. J. *J. Am. Chem. Soc.* **2000**, *122*, 6299.

(15) 56 kcal/mol excess vibrational energy will distribute among kinetic and potential energy according to the virial theorem, so as to have the same values for the mean kinetic ($\langle T \rangle$) and the mean potential ($\langle V \rangle$) energy. Thus, $\langle T \rangle = \langle V \rangle = 28$ kcal/mol. The kinetic energy will flow among all the 24 degrees of freedom of the molecule, thus giving a mean value $\langle T_d \rangle$ of 1.6 kcal/mol for each mode. This corresponds to a mean temperature **T** of about 900 °C according to the formula $\boldsymbol{T} = 2\langle T_d \rangle / K_b$, where K_b is the Boltzmann constant. Of course, our simulated ensemble is microcanonical.

(16) Köppel, H.; Domcke, W.; Cederbaum, L. S. In *Adv. Chem. Phys*; Prigogine, I., Rice, S. A., Eds.; John Wiley & Sons: New York, 1984; Vol. 57, pp 59−246.

(17) (a) Preston, R. K.; Tully, J. C. *J. Chem. Phys.* **1971**, *54*, 4297. (b) Tully, J. C. Preston, and, R. K. *J. Chem. Phys.* **1971**, *55*, 562.

(18) (a) Bernardi, F.; Olivucci, M.; McDouall, J. J. W.; Robb, M. A. *J. Chem. Phys.* **1988**, *89*, 6365. (b) Vreven, T.; Bernardi, F.; Garavelli, M.; Olivucci, M.; Robb, M. A. Schlegel, H. B.; *J. Am. Chem. Soc.* **1997**, *119*, 12 687−12 688.

(19) Deyerl, H. J.; Fischer, I.; Chen, P. *J. Chem. Phys.* **1999**, *104*, 1450 and private communication.

(20) A viscosity scaling factor (*S*) is used to simulate viscosity. At each step of the trajectory, the gradient vector (**g**) is adjust according to the following relation (i.e. Stokes Law): $\mathbf{g} = \mathbf{g} + S_*\mathbf{m}$ where **m** is the momentum vector and *S* has values in the range from 0 to 0.05.

(21) Even with very small perturbations (i.e., very small values for the viscosity factor *S*, see ref 20), τ_{S_1} is dramatically reduced. This has been proved via restarting a bunch (∼30) of randomly selected trajectories at different (and small) *S* values. In particular, a scaling factor value of 0.006 drops τ_{S_1} down to 200 fs (subpicosecond time scale) as it is expected experimentally. Concurrently, QY for the $\mathbf{1} \rightarrow \mathbf{1_{E,E\rightarrow Z,Z}}$ process invariably decreases and the rotation about the central single bond is hindered thus reducing the difference with the experimental data shown in Table 2.

(22) (a) Rejto, P. A.; Bindewald, E.; Chandler, D. *Nature* **1995**, *375*, 129−131. (b) Liu, Q.; Wang, J.-K.; Zewail, A. H. *J. Phys. Chem.* **1995**, *99*, 11 321.

(23) (a) Jimenez, R.; Fleming, G. R.; Kumar, P. V.; Maroncelli, M. *Nature* **1994**, *369*, 471−473 (b) Liu, Q.; Wang, J.-K.; Zewail, A. H. *J. Phys. Chem.* **1995**, *99*, 11 309. (c) Heikal, A. A.; Chong, S. H.; Baskin, J. S.; Zewail, A. H. *Chem. Phys. Lett.* **1995**, *242*, 380−389. (d) Zhong, Q.; Wang, Z.; Sun, Y.; Zhu, Q.; Kong, F. *Chem. Phys. Lett.* **1996**, *248*, 277−282.

(24) Garavelli, M.; Celani, P.; Fato, M.; Bearpark, M. J.; Smith, B. R.; Olivucci, M.; Robb, M. A. *J. Phys. Chem. A.* **1997**, *101*, 2023.

(25) Garavelli, M.; Smith, B. R.; Bearpark, M. J.; Bernardi, F.; Olivucci, M.; Robb, M. A. *J. Am. Chem. Soc.* **2000**, *122*, 5568.